

All-Orders Resummation of Leading Logarithmic Contributions to Heavy Quark Production in Polarized $\gamma\gamma$ Collisions

Michael Melles^{1*} and W. James Stirling^{1,2†}

- 1) Department of Physics, University of Durham, Durham DH1 3LE, U.K.
- 2) Department of Mathematical Sciences, University of Durham, Durham DH1 3LE, U.K.

Abstract

The measurements of the $\gamma\gamma$ and $b\bar{b}$ partial decay widths of an intermediate-mass Standard Model Higgs boson are among the most important goals of a future photon linear collider. While in an initially polarized $J_z = 0$ state the background process $\gamma\gamma \rightarrow b\bar{b}$ is suppressed by $\frac{m_b^2}{s}$, radiative corrections remove this suppression and are known to be very sizable at the one-loop level. In particular a new type of purely hard double logarithmic (DL) correction can even make the cross section negative at this order in perturbation theory. The second order term of the series is also known and enters with a positive sign at the two loop level. From a theoretical as well as a practical point of view it is clearly desirable to resum this series and to know its high energy behavior. In this paper, we derive the series of these novel “non-Sudakov” logarithms to all orders and calculate the high energy limit analytically. We also give explicit three loop corrections in the DL-approximation as a check of our results and show that the three loop structure also reveals the higher order behavior of mixed hard and

*Michael.Melles@durham.ac.uk

†W.J.Stirling@durham.ac.uk

soft double logarithms. We are thus able to resum the virtual DL-corrections to $\gamma\gamma(J_z = 0) \rightarrow b\bar{b}$ to all orders.

1 Introduction

Among the many important physics processes which can be studied at a future high-energy photon linear collider (PLC) [1, 2, 3], the production of Higgs bosons, $\gamma\gamma \rightarrow H$, stands out. In particular, identification of an intermediate-mass Standard Model Higgs boson via its (dominant) $H \rightarrow b\bar{b}$ decay channels seems feasible and would provide an important measurement of the $\gamma\gamma$ and $b\bar{b}$ partial decay widths.

The dominant (continuum) background to $\gamma\gamma \rightarrow H \rightarrow b\bar{b}$ comes from the Standard Model processes $\gamma\gamma \rightarrow c\bar{c}, b\bar{b}$. Various techniques can be used to suppress these. The most effective appears to be to *polarize* the initial-state photons: Higgs bosons are only produced from an initial state with $J_z = 0$, whereas the leading-order $q\bar{q}$ ($q = c, b$) backgrounds are dominantly produced from the $J_z = \pm 2$ initial state. More precisely, production from the $J_z = 0$ state is suppressed by m_q^2/s [4, 5, 6]. Hence in the region of the Higgs resonance $\sigma_{q\bar{q}}(J_z = 0)/\sigma_{q\bar{q}} \sim m_q^2/M_H^2$ and the $c\bar{c}$ and $b\bar{b}$ backgrounds are heavily suppressed.

Unfortunately, the $\mathcal{O}(m_q^2)$ suppression of the $J_z = 0$ background does not survive beyond leading order in QCD perturbation theory. In particular, there is no corresponding mass suppression of the $\mathcal{O}(\alpha_s)$ $\gamma\gamma \rightarrow q\bar{q}g$ $J_z = 0$ amplitude squared. Although this gives rise notionally to three-jet configurations, in certain circumstances (for example, collinear $\gamma \rightarrow q\bar{q}$ splitting followed by $\gamma q \rightarrow qg$ Compton scattering) these can mimic the two-jet Higgs $\rightarrow b\bar{b}$ signal. Of course a combination of b -tagging of both jets and three-jet veto can *in principle* eliminate the bulk of this background, and one is left considering the perturbative corrections from virtual and soft real gluon emission. These have the same $\mathcal{O}(m_q^2/s)$ suppression as the leading-order contribution¹ However the perturbation series now contains large double logarithmic corrections $\sim \alpha_s^n \log^{2n}(s/m_q^2)$ at each order n , which potentially can give sizable corrections. Apart from their phenomenological importance, these logarithms are of theoretical interest. They do not have an obvious ‘Sudakov’ exponentiating behavior, arising from the fact that they originate in non-trivial regions of soft gluon phase space. Furthermore, for any particular virtual gluon diagram they are mixed up with the genuine infra-red logarithms $\sim \alpha_s^n \log^n(m_q^2/\lambda^2) \log^n(m_q^2/s)$, where λ is a fictitious gluon mass introduced to control the soft divergences.

In Ref. [7] the double logarithmic contributions were studied in considerable detail through two loops, i.e. up to and including $\mathcal{O}(\alpha_s^2 \log^4(s/m_q^2))$ contributions. Inspection of the one- and two-loop coefficients led to the claim that, for $m_q = m_b$ and $\sqrt{s} \simeq M_H$, the perturbation series was reasonably well approximated by the lowest two orders. However from both a theoretical and practical point of view it is clearly desirable to have more information about the behavior of the double-logarithmic (DL) terms to all orders, in particular to see if resummation is possible. This is the goal of the present

¹Unless otherwise stated, from now on all statements about amplitudes and cross sections will refer to the $J_z = 0$ helicity projection.

paper. As we shall see, a careful study of all the relevant two- and three-loop diagrams *does* reveal the pattern of the DL terms, and allows the all-orders result to be derived and resummed.

In this paper we shall restrict ourselves to the theoretical study of the origin and calculation of the DL terms. In a future paper we will investigate their numerical effect on realistic PLC cross sections. We begin, in section 2, by deriving the leading order result for the $J_z = 0$ cross section, identifying the origin of the $\mathcal{O}(m_q^2)$ suppression. In section 3 we discuss the structure of the one-loop corrections, show how the DL contributions arise, and compare these with the known one loop result [5, 6, 7]. The main part of the paper is section 4, where we calculate all three-loop DL contributions and deduce the all-orders result. Section 5 contains a summary of our results.

2 The Born Amplitude

We begin with a rederivation of the underlying Born process. Recall that for an initial state with $J_z = 0$ the cross section vanishes in the massless limit. In other words, the background to the standard Higgs production process via a fermion loop and subsequent decay into a $b\bar{b}$ or $c\bar{c}$ final state is suppressed by a factor of $\frac{m_q^2}{s}$. Higher order radiative (Bremsstrahlung) corrections remove this suppression in principle [4]. One therefore needs to keep at least terms of $\mathcal{O}\left(\frac{m_q}{\sqrt{s}}\right)$ in the calculation of the Born amplitudes shown in Fig. 1. We are also only interested in the region of large scattering angle θ , which is the dominant event topology of the Higgs signal [5, 7].

Keeping only terms of $\mathcal{O}\left(\frac{m_q}{\sqrt{s}}\right)$, we find it convenient to separate out the mass dependence of the spinors according to [8]

$$u^\mu(p) = \frac{\not{p} + m}{\sqrt{2p \cdot q}} |q, -\mu\rangle \quad (1)$$

$$v^\mu(p) = \langle q, -\mu | \frac{-\not{p} + m}{\sqrt{2p \cdot q}} \quad (2)$$

where the spinors on the r.h.s. are massless and q is an arbitrary reference four-momentum with $q^2 = 0$. The separation of the mass terms then allows for the convenient usage of the polarization vector [8]

$$\varepsilon_\nu^\lambda(k, h) \equiv \frac{1}{\sqrt{4k \cdot h}} \langle k, \lambda | \gamma_\nu | h, \lambda \rangle \quad (3)$$

$$\not{\varepsilon}^\lambda(k, h) = \frac{2}{\sqrt{4k \cdot h}} (|k, -\lambda\rangle \langle h, -\lambda| + |h, \lambda\rangle \langle k, \lambda|) \quad (4)$$

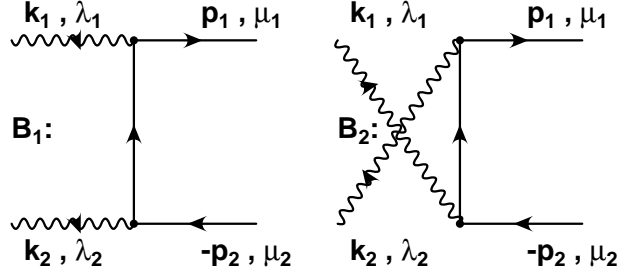


Figure 1: The Born process in polarized $\gamma + \gamma \rightarrow q + \bar{q}$ with the notation of momenta used in the remainder of this work. Keeping only the mass term in the numerator of the fermion propagator gives the correct Born result only for $\theta \approx 0^\circ$. Details are given in the text.

where here we denote the arbitrary massless reference momentum by h . In the following we will also use simply m for an arbitrary fermion mass, as the results derived do not depend on any heavy quark approximation. It is understood that for any application, the relevant fermion masses for the background to Higgs production below the W^+W^- threshold are the b - and c -quark masses. The cross section of the latter is enhanced by a relative factor of 16 from the different charges of the quarks.

Using the above notation we find for the Born amplitude $\mathcal{M}_{Born} \equiv B_1 + B_2$ with an initial $J_z = 0$ state:

$$\mathcal{M}_{Born} = \frac{8me^2Q^2\delta_{\lambda_1,\lambda_2}\delta_{\mu_1,\mu_2}\delta_{\lambda_1,\mu_1}}{\sqrt{s}(1 - \beta^2 \cos^2 \theta)} \quad (5)$$

with $\beta = \sqrt{1 - \frac{4m^2}{s}}$, e the electromagnetic coupling with magnitude Q and θ the scattering angle. The Kronecker- δ 's allow for a non-zero contribution only in case all four helicities are the same. The result agrees with Refs. [7, 5] up to $\mathcal{O}\left(\frac{m}{\sqrt{s}}\right)$ and displays the somewhat surprising feature of a bosonic angular dependence (as in Bhabha scattering for instance), with no θ -terms in the numerator.

This feature leads one to suspect that by keeping only the mass term of the virtual fermion propagator, one should obtain Eq. 5 very easily. A detailed analysis of this contribution, however, yields:

$$\begin{aligned} \mathcal{M}_{Born}^m = & \frac{4me^2Q^2\delta_{\lambda_1,\lambda_2}\delta_{\mu_1,\mu_2}}{s(1 - \beta^2 \cos^2 \theta)} \left[\langle k_1, -\lambda_1 | k_2, \lambda_1 \rangle (1 + \beta^2 \cos^2 \theta) \delta_{\lambda_1,\mu_1} + \right. \\ & \left. \langle k_1, \lambda_1 | k_2, -\lambda_1 \rangle (1 - \beta^2 \cos^2 \theta) \delta_{-\lambda_1,\mu_1} \right] \quad (6) \end{aligned}$$

While it does not agree with the exact result in Eq. 5, it is also evident that for small angles and high energies both solutions do agree. It was found in Ref. [7] that this feature holds also through one and two loops if one is interested only in the leading logarithmic accuracy at large angles. The reason for this seemingly contradictory

behavior is that while the angle between the outgoing fermion (antifermion) and the beamline is large, the angle between the incoming photon and the emitted soft parton is small. Therefore, while it is wrong to keep only the m -term in the propagator of the virtual fermion for the Born amplitude, it actually *does* give the correct leading logarithmic structure of higher order contributions with a soft fermion line.

For higher order corrections it is also convenient to use the following expression for the $J_z = 0$ \mathcal{M}_{Born} amplitude:

$$\mathcal{M}_{Born} \approx -\frac{8me^2Q^2}{s \sin^2\theta} \varepsilon_1^{-\lambda}{}_{\nu}(k_1, k_2) \varepsilon_2^{-\lambda\nu}(k_2, k_1) \langle p_1, \lambda | p_2, -\lambda \rangle \quad (7)$$

In the following we describe how to obtain the double logarithms in the one loop approximation and introduce the techniques applied in the later stages of the paper.

3 One Loop Form Factors

At the one loop level, the only diagram that can contribute large double logarithms is the box diagram with a virtual gluon connecting the outgoing $q\bar{q}$ pair. While the general method of employing Sudakov parametrizations and integrating over the perpendicular components of soft loop momenta is well known [9] and has been used extensively [10, 11, 12, 13], we still find it useful to briefly review some basic properties. In section 4 we will also remark on some subtleties one encounters with higher order virtual corrections.

Large logarithms occur only when there are small and large scales connected in a Feynman diagram. While the particular Feynman diagram is gauge dependent, the leading logarithmic contribution is not. In our case, the box diagram is connected with vertex and self energy corrections to form a gauge invariant cross section. However, in any gauge only the four-point diagram can yield the desired pair of large logarithms. It is therefore independent of the particular choice of gauge. A familiar and analogous example of the same mechanism is the gauge invariance of the infra red $\frac{1}{\epsilon}$ term in the context of dimensional regularization for a massless box diagram.

In Fig. 2 we list the four distinct topologies that allow a doubly logarithmic contribution from the box diagram. The “blob” always denotes a hard momentum flowing through the omitted propagator and in each case there is a corresponding soft momentum flowing through the propagator facing the hard blob.

The feature which makes this process interesting and very different from the standard Sudakov form factor is the fact that we have soft *fermion* contributions as well. “Soft” means in this context soft compared to the hard blob.

The Sudakov decomposition of loop momenta should be chosen such that the external four momenta joining the soft parton line are used as the base vectors.² For

²In higher orders this is not always unambiguous, as we will discuss in section 4 and can lead to technical difficulties.

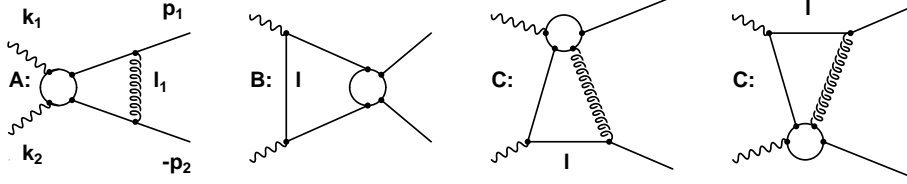


Figure 2: The one loop soft and hard topologies contributing to the doubly logarithmic form factors. These graphs are obtained from the one loop box diagram. We denote the soft topology as \mathcal{A} , the first hard topology as \mathcal{B} and the second (third) as \mathcal{C} .

the graphs of Fig. 2, however, we take:

$$\text{topology } \mathcal{A} : l_{\perp} \equiv \beta_1 \left(p_1 - \frac{m^2}{s} p_2 \right) + \alpha_1 \left(p_2 - \frac{m^2}{s} p_1 \right) + l_{\perp} \quad (8)$$

$$\text{topology } \mathcal{B} : l \equiv \beta k_1 + \alpha k_2 + l_{\perp} \quad (9)$$

$$\text{topology } \mathcal{C} : l \equiv \beta k_2 + \alpha \left(p_2 - \frac{m^2}{s} k_2 \right) + l_{\perp} \quad (10)$$

At large angles and in the doubly logarithmic (DL) approximation, we have

$$2p_1 \cdot k_1 = 2p_2 \cdot k_2 \approx 2p_1 \cdot k_2 = 2p_2 \cdot k_1 \approx 2p_1 \cdot p_2 \approx 2k_1 \cdot k_2 = s \quad (11)$$

The phase space for the large logarithms is given by

$$1 \gg |\alpha|, |\beta| \gg |l_{\perp}^2/s|, \gg |m^2/s| \quad (12)$$

$$1 \gg |\alpha_i|, |\beta_i| \gg |l_{i\perp}^2/s| \gg |\lambda^2/s| \quad (13)$$

where we already have multiple gluon insertions in mind. The four dimensional Minkowski measure is rewritten according to $d^4l = d^2l_{\perp} d^2l_{\parallel}$, with

$$d^2l_{\perp} = |l_{\perp}| d|l_{\perp}| d\phi = \frac{1}{2} dl_{\perp}^2 d\phi = \pi dl_{\perp}^2 \quad (14)$$

$$d^2l_{\parallel} = |\partial(l_0, l_x)/\partial(\alpha, \beta)| d\alpha d\beta \approx \frac{s}{2} d\alpha d\beta \quad (15)$$

The integrations over the transverse momenta of the soft particles is performed by taking half of the residues in the corresponding propagators:

$$\frac{d^4l}{l^2 - m^2 + i\epsilon} = \frac{s}{2} \frac{d\alpha d\beta d^2l_{\perp}}{s\alpha\beta + l_{\perp}^2 - m^2 + i\epsilon} \longrightarrow -i\pi^2 \frac{s}{2} d\alpha d\beta \Theta(s\alpha\beta - m^2) \quad (16)$$

$$\frac{d^4l_i}{l_i^2 - \lambda^2 + i\epsilon} = \frac{s}{2} \frac{d\alpha_i d\beta_i d^2l_{i\perp}}{s\alpha_i\beta_i + l_{i\perp}^2 - \lambda^2 + i\epsilon} \longrightarrow -i\pi^2 \frac{s}{2} d\alpha_i d\beta_i \Theta(s\alpha_i\beta_i - \lambda^2) \quad (17)$$

The DL-contribution of a particular Feynman diagram is thus given by

$$\mathcal{M}_k = \mathcal{M}_{Born} \mathcal{F}_k \quad (18)$$

where the \mathcal{F}_k are given by integrals over the remaining Sudakov parameters at the n -loop level:

$$\text{topology } \mathcal{A} \quad : \quad \mathcal{F}_k = \left(\frac{\alpha_s}{2\pi}\right)^n \prod_{i=1}^n \int_0^1 \int_0^1 \frac{d\alpha_i}{\alpha_i} \frac{d\beta_i}{\beta_i} \Theta_k \quad (19)$$

$$\text{topology } \mathcal{B}, \mathcal{C} \quad : \quad \mathcal{F}_k = \left(\frac{\alpha_s}{2\pi}\right)^n \int_0^1 \int_0^1 \frac{d\alpha}{\alpha} \frac{d\beta}{\beta} \prod_{i=1}^{n-1} \int_0^1 \int_0^1 \frac{d\alpha_i}{\alpha_i} \frac{d\beta_i}{\beta_i} \Theta_k \quad (20)$$

The factors Θ_k are specific to the given Feynman diagram and contain its color factors and the restrictions on the occurring Sudakov variables necessary to ensure that the matrix element has logarithmic behavior in each of them. The range of integration is restricted by demanding that there is at least one pole term on the opposite side of the contour of integration from the other propagator terms, since Cauchy's Theorem would otherwise give a vanishing contribution.

As a simple example, we now apply the above techniques to the one loop diagrams of Fig. 2. For the standard infrared form factor of topology \mathcal{A} the Sudakov phase space is schematically given in Fig. 3 and leads to the following result:

$$\begin{aligned} \mathcal{F}_{\mathcal{A}} &= -C_F \frac{\alpha_s}{2\pi} \int_0^1 \int_0^1 \frac{d\alpha_1}{\alpha_1} \frac{d\beta_1}{\beta_1} \Theta(s\alpha_1\beta_1 - \lambda^2) \Theta\left(\alpha_1 - \frac{m^2}{s}\beta_1\right) \Theta\left(\beta_1 - \frac{m^2}{s}\alpha_1\right) \\ &= -C_F \frac{\alpha_s}{2\pi} \left[\int_{\frac{\lambda^2}{s}}^{\frac{\lambda}{m}} \frac{d\beta_1}{\beta_1} \int_{\frac{\lambda^2}{s\beta_1}}^1 \frac{d\alpha_1}{\alpha_1} + \int_{\frac{\lambda}{m}}^1 \frac{d\beta_1}{\beta_1} \int_{\frac{m^2}{s}\beta_1}^1 \frac{d\alpha_1}{\alpha_1} - \int_{\frac{\lambda^2}{s}}^{\frac{\lambda m}{s}} \frac{d\beta_1}{\beta_1} \int_{\frac{\lambda^2}{s\beta_1}}^1 \frac{d\alpha_1}{\alpha_1} \right. \\ &\quad \left. - \int_{\frac{\lambda m}{s}}^{\frac{m^2}{s}} \frac{d\beta_1}{\beta_1} \int_{\frac{s}{m^2}\beta_1}^1 \frac{d\alpha_1}{\alpha_1} \right] \\ &= -C_F \frac{\alpha_s}{2\pi} \left(\frac{1}{2} \log^2 \frac{m^2}{s} + \log \frac{m^2}{s} \log \frac{\lambda^2}{m^2} \right) \end{aligned} \quad (21)$$

The result is identical to the usual DL-Sudakov form factor [14]. For the hard form factors of topologies \mathcal{B} and \mathcal{C} we have analogously:

$$\begin{aligned} \mathcal{F} &\equiv \mathcal{F}_{\mathcal{B}} = \mathcal{F}_{\mathcal{C}} = -C_F \frac{\alpha_s}{2\pi} \int_0^1 \int_0^1 \frac{d\alpha}{\alpha} \frac{d\beta}{\beta} \Theta(s\alpha\beta - m^2) \\ &= -C_F \frac{\alpha_s}{4\pi} \log^2 \frac{m^2}{s} \end{aligned} \quad (22)$$

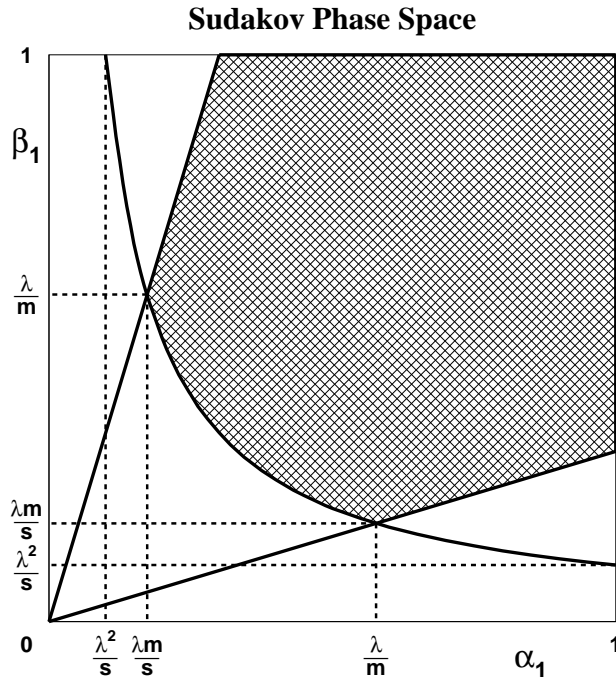


Figure 3: The one loop soft Sudakov phase space of topology \mathcal{A} . The Θ -functions given in Eq. 21 are translated into integrals covering the shaded area in the figure for the Sudakov parameters α_1 and β_1 as defined in Eq. 8. At higher orders, the phase space becomes increasingly untrackable and even numerical integrations need many iterations in order to converge.

Taken together, and noting that topology \mathcal{C} has a multiplicity factor 2, we thus have rederived the one loop structure of Refs. [5, 6] and [7] in the DL-approximation. The fact that the Born amplitude factors out is trivial for topology \mathcal{A} . For topologies \mathcal{B} and \mathcal{C} the exact numerator factorization was derived in Ref. [7]. In the former, it is connected with the aforementioned purely bosonic angular dependence of \mathcal{M}_{Born} of Eq. 5, as it contains a hard subprocess $q + \bar{q} \rightarrow q + \bar{q}$. In the latter, one needs to exploit the Dirac equation and gauge invariance in order to factor out the hard subprocess $\gamma + q \rightarrow q + g$ and the Born amplitude. Details are given in [7].

With these results, we can now proceed to investigate the higher order structure of the leading logarithmic corrections from insertions of multiple gluons in the basic contributions shown in Fig. 2. The next section gives explicit results through three loops which enable us to arrive at an all orders resummation of both hard as well as soft logarithmic corrections.

4 All Orders Resummation

In this section we derive the expressions for the leading logarithmic corrections to all orders for the $J_z = 0$ initial state $\gamma + \gamma \rightarrow q + \bar{q}$ process. While it is possible to rigorously derive these corrections to all orders for topologies \mathcal{A} and \mathcal{B} , for topology \mathcal{C} only the new hard “non-Sudakov” logarithms can be treated analytically. For soft insertions we derive explicit three loop results and show that essentially the same factorization structure emerges as in \mathcal{B} . This behavior is then extrapolated to all orders.

At this point we note that we have recalculated the virtual two loop corrections presented in Ref. [7] and agree with their results. In the following, we therefore restrict ourselves to a discussion of the three loop level. All resummed formulae were checked explicitly through one-, two- and three-loops.

4.1 The Sudakov Form Factor

We begin with the Sudakov form factor of topology \mathcal{A} . At three loops, the relevant Feynman diagrams are given in Fig. 12. The summation is analogous to the soft vertex corrections where the exponentiation to all orders for a color singlet final state was proved in Ref. [15] to leading order by employing an asymptotic Hamiltonian as well as the coherent state formalism. Explicit three loop calculations were performed in the leading logarithmic approximation in Ref. [16] and related work can also be found in Refs. [17, 18]. For all orders corrections to topology \mathcal{A} we thus find the familiar result:

$$\mathcal{F}^{soft} = \exp(\mathcal{F}_{\mathcal{A}}) \quad (23)$$

The non-Abelian color factors of diagrams with an “Abelian” topology are canceled by the contributions of the purely non-Abelian topologies. In this context it is worth noting that for the three gluon vertex coupling, there is an effective factor of $-\frac{1}{2}$ stemming from two contributions in numerator terms that are needed to obtain the required number of logarithms. This is only the case if one has a denominator of the type $\frac{1}{(l-l_i)^2}$. For one gluon very soft, there is a term $-2l_i \cdot p$ and one $l_i \cdot p$, l_i being the other (relatively) soft gluon momentum and p an external hard fermion momentum. The Lorentz structure of the three gluon vertex is such that only these two terms give DL-contributions (the third connects the same fermion line). The effective soft contribution is therefore $-l \cdot p$, compared with a factor $2p_\nu$ from the emission of a soft gluon off a fermion line.

4.2 Resummation of Novel Hard Logarithms

The interesting feature of the higher order corrections to the one-loop diagrams of Fig. 2 is that there are novel purely hard “non-Sudakov” logarithms due to the presence of

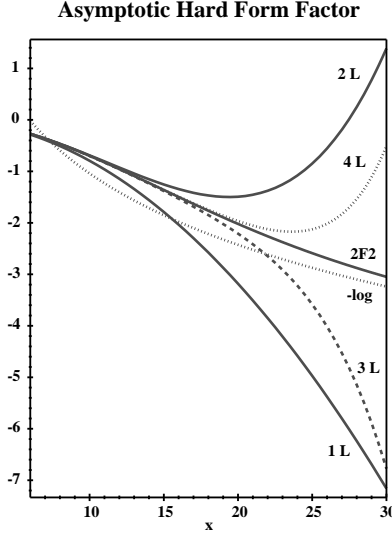


Figure 4: A comparison of the exact summed result of Eq. 24 with the asymptotic form given in Eq. 26 and the first four terms in the expansion. The value of the coupling was kept fixed at $\alpha_s = 0.1$ and $x = \log \frac{s}{m^2}$. At a fixed order in perturbation theory the high energy limit alternates. Only the exact and asymptotic form factors can be seen to give the correct limit at high energies.

the “soft” fermion line in topologies \mathcal{B} and \mathcal{C} . In the case where a gluon insertion does not end on an external (hard) fermion line, the soft fermion line serves essentially as a cutoff for gluons that are soft compared to the hard blob. The diagrams are listed in Figs. 13 and 14 and denoted by h_i , as they contain no soft Sudakov contributions. Besides a different color factor, both contributions are identical and lead to the same structure as in the soft case, except for the last two integrations. They have the additional effect of eliminating $\Theta\left(\alpha_i - \frac{m^2}{s}\beta_i\right)$ terms, which are very important in the soft case (see Fig. 3). The reason is simply that they are automatically fulfilled since the soft fermion line induces a $\frac{m^2}{s}$ cutoff for the soft gluon Sudakov variables. The integrations over the gluonic variables can thus be performed easily and summing over i gluon insertions we have:

$$\begin{aligned}
\mathcal{F}^{hard} &\sim \sum_{i=0}^{\infty} \left(\frac{\alpha_s}{2\pi}\right)^{i+1} \int_{\frac{m^2}{s}}^1 \frac{d\beta}{\beta} \int_{\frac{m^2}{s\beta}}^1 \frac{d\alpha}{\alpha} \frac{(-1)^{i+1}}{i!} \log^i \beta \log^i \alpha \\
&= \sum_{i=0}^{\infty} \left(\frac{\alpha_s}{2\pi}\right)^{i+1} \frac{(-1)^i}{(i+1)!} \int_{\frac{m^2}{s}}^1 \frac{d\beta}{\beta} \log^i \beta \left(\log \frac{m^2}{s\beta}\right)^{i+1}
\end{aligned}$$

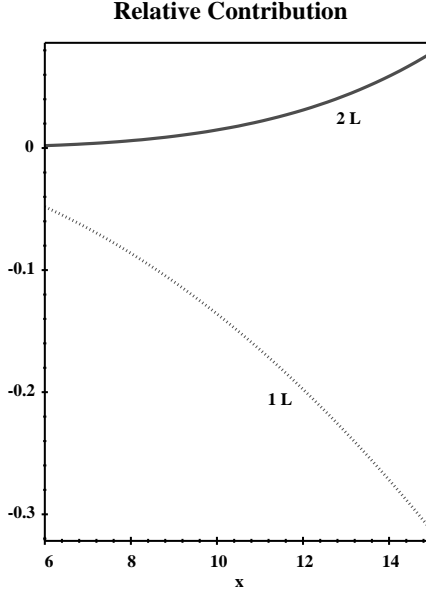


Figure 5: The relative contribution of the one (1L) and two (2L) loop corrections to the exact summed result of Eq. 24. The value of the coupling was kept fixed at $\alpha_s = 0.1$ and $x = \log \frac{s}{m^2}$. For the b-quark mass, $\sqrt{s} = 100$ GeV corresponds roughly to $x = 6.2$, $\sqrt{s} = 1$ TeV to $x = 10.8$. In case of the c-quark, $\sqrt{s} = 100$ GeV corresponds roughly to $x = 8.4$, $\sqrt{s} = 1$ TeV to $x = 13$. The higher than second order corrections are thus important whenever the experimental accuracy reaches the percentile level.

Using partial integration i -times (differentiating $\log^{i+1} \frac{m^2}{s\beta}$, integrating $\frac{\log^i \beta}{\beta}$), we find:

$$\begin{aligned}
\mathcal{F}^{hard} &\sim \sum_{i=0}^{\infty} \left(\frac{\alpha_s}{2\pi}\right)^{i+1} \frac{(-1)^i (i+1)!}{(i+1)! (i+1) \dots 2i} \int_{\frac{m^2}{s}}^1 \frac{d\beta}{\beta} \log^{2i} \beta \log \frac{m^2}{s\beta} \\
&= \sum_{i=0}^{\infty} \left(\frac{\alpha_s}{2\pi}\right)^{i+1} \frac{(-1)^i \Gamma(i+1)}{\Gamma(2i+1)} \left[\frac{1}{2i+1} \log^{2i+1} \beta \log \frac{m^2}{s} - \frac{1}{2i+2} \log^{2i+2} \beta \right]_{\frac{m^2}{s}}^1 \\
&= - \sum_{i=0}^{\infty} \left(\frac{\alpha_s}{2\pi}\right)^{i+1} \frac{(-1)^i \Gamma(i+1)}{\Gamma(2i+3)} \log^{2i+2} \frac{m^2}{s} \\
&= -\frac{\alpha_s}{4\pi} \log^2 \frac{m^2}{s} {}_2F_2\left(1, 1; 2, \frac{3}{2}; -\frac{\alpha_s}{8\pi} \log^2 \frac{m^2}{s}\right) \tag{24}
\end{aligned}$$

In order to compare this result with the known one- and two-loop leading logarithmic results we list them below explicitly and find agreement with Refs. [5, 6, 7]:

$$\begin{aligned} \mathcal{F}^{hard} \sim & -\frac{1}{2} \left(\frac{\alpha_s}{2\pi}\right) \log^2 \frac{m^2}{s} + \frac{1}{24} \left(\frac{\alpha_s}{2\pi}\right)^2 \log^4 \frac{m^2}{s} - \frac{1}{360} \left(\frac{\alpha_s}{2\pi}\right)^3 \log^6 \frac{m^2}{s} \\ & + \mathcal{O}\left(\left(\frac{\alpha_s}{2\pi}\right)^4\right) \end{aligned} \quad (25)$$

The asymptotic behavior of the hypergeometric function ${}_2F_2$ for $s \rightarrow \infty$ can be obtained by using an integral representation [19] and taking the leading pole term. In our case we find

$$\begin{aligned} \mathcal{F}^{hard} \sim & -\frac{\alpha_s}{4\pi} \log^2 \frac{m^2}{s} \Gamma\left(\frac{3}{2}\right) \int_{-i\infty}^{i\infty} \frac{dt}{2\pi i} \frac{\Gamma^2(1+t) \Gamma(-t)}{\Gamma(2+t) \Gamma\left(\frac{3}{2}+t\right)} \left(\frac{\alpha_s}{8\pi} \log^2 \frac{m^2}{s}\right)^t \\ \xrightarrow{s \rightarrow \infty} & -\log\left(\frac{\alpha_s}{\pi} \log^2 \frac{m^2}{s}\right) \end{aligned} \quad (26)$$

The last line follows from the residue of the integral representation at $t = -1$, closing the contour in the negative t -plane. All higher negative pole contributions are suppressed by at least a factor of $\frac{1}{\log^2 \frac{m^2}{s}}$. With the $\frac{m}{\sqrt{s}}$ suppression contained in the Born amplitude (5), the high energy limit is well behaved.

It is also possible to reconstruct the asymptotic series based on the above integral representation. The higher order poles are simple ones and can thus be evaluated easily. We find

$$\begin{aligned} \mathcal{F}^{hard} \sim & -\frac{\alpha_s}{4\pi} \log^2 \frac{m^2}{s} \Gamma\left(\frac{3}{2}\right) \int_{-i\infty}^{i\infty} \frac{dt}{2\pi i} \frac{\Gamma^2(1+t) \Gamma(-t)}{\Gamma(2+t) \Gamma\left(\frac{3}{2}+t\right)} \left(\frac{\alpha_s}{8\pi} \log^2 \frac{m^2}{s}\right)^t \\ = & -\gamma - \log\left(\frac{\alpha_s}{2\pi} \log^2 \frac{m^2}{s}\right) + \sum_{n=2}^{\infty} \frac{2^n}{(n-1)\pi} \frac{\Gamma\left(\frac{3}{2}\right) \Gamma\left(n - \frac{1}{2}\right)}{\left(\frac{\alpha_s}{4\pi} \log^2 \frac{m^2}{s}\right)^{n-1}} \end{aligned} \quad (27)$$

Although it possesses the ominous factorial growth of the coefficients in the series for the higher order residue contributions, the equivalent original expansion in terms of the confluent hypergeometric function in Eq. 24 means that it is Borel summable and that the high energy limit in Eq. 26 does indeed give the correct behavior for $s \rightarrow \infty$. Fig. 4 contains a comparison of the exact hard form factor of Eq. 24 and its asymptotic logarithmic divergence given by the first term in Eq. 27. They can be seen to agree in the high energy limit. In addition the figure demonstrates that at a fixed order in perturbation theory, the result alternates between $\pm\infty$ for high energies.

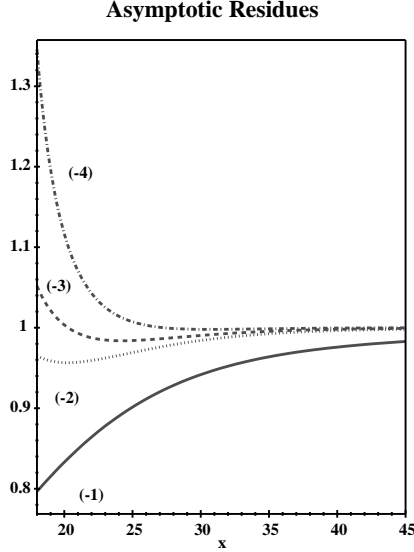


Figure 6: A ratio of the first four residues of the integral representation of Eq. 27 with the exact result of Eq. 24. The value of the coupling was kept fixed at $\alpha_s = 0.1$ and $x = \log \frac{s}{m^2}$. At lower energies the $\frac{1}{\log^2 \frac{m^2}{s}}$ divergences of the higher order residues is clearly visible. At high energies, however, they can be seen to give the correct limit.

The numerical effect of the higher order terms is shown in Fig. 5 where the all orders hard form factor is compared to the one- and two-loop corrections at realistic future collider energies. As explained in the figure, only if the experimental accuracy reaches the percentile level are higher than second order contributions important. The relative size of the all orders correction is larger for $m = m_c$ than for the b-quark mass.

A more detailed comparison of the behavior of the higher order residues is given in Fig. 6. The first four pole contributions are plotted against the exact hard form factor and agree with Eq. 24 in the asymptotic regime. At lower energies the $\frac{1}{\left(\log^2 \frac{m^2}{s}\right)^n}$ behavior of the first three simple residues of Eq. 27 is clearly visible.

In order to check this derivation explicitly at the three loop level, we have calculated the corresponding diagrams denoted by h in Figs. 13 and 14 and find the following results (modulo color factors and choosing for the Sudakov decomposition $\{k_1, k_2\}$ for topology \mathcal{B} and $\{k_2, (p_2 - \frac{m^2}{s}k_2)\}$ for topology \mathcal{C}):

$$\Theta_{h_1} \sim \Theta(s\alpha\beta - m^2) \Theta(\alpha_2 - \alpha_1) \Theta(\alpha_1 - \alpha) \Theta(\beta_2 - \beta_1) \Theta(\beta_1 - \beta) \quad (28)$$

$$\Theta_{h_2} \sim \Theta(s\alpha\beta - m^2) \Theta(\alpha_1 - \alpha_2) \Theta(\alpha_2 - \alpha) \Theta(\beta_2 - \beta_1) \Theta(\beta_1 - \beta) \quad (29)$$

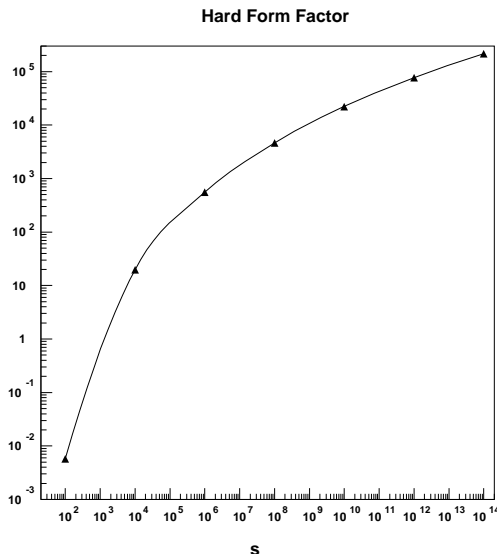


Figure 7: A comparison of the third term of the series expansion in Eq. 24 (line) and the explicit three loop results given in Eqs. 28 and 29 (triangles). For the three loop data we used 10^6 evaluations for each of the 100 iterations of the Monte Carlo integrator VEGAS [20]. $m_b = 4.5$ GeV was used in both results. The absolute values are plotted and the agreement is below the percent level. Color factors and the coupling constant are omitted.

The remaining terms h_3 and h_4 in each figure cancel the non-Abelian color factor stemming from the crossed box insertion h_2 , i.e. $h_3 = h_4 \sim \frac{h_2}{2}$. It can easily be seen from the explicit form in Eqs. 28 and 29 that the contributions of the gluon insertions are cut off effectively by the fermion line Sudakov variables for which $\frac{m^2}{s}$ is the minimum value attainable.

Fig. 7 contains a comparison of the explicit three loop results given by $h_1 + h_2$ and the third term in the series 24. The agreement is below the percentile level.

For completeness, we give the form factors explicitly for the two topologies \mathcal{B} and \mathcal{C} below, including the coupling and their differing color structure:

$$\mathcal{F}_{\mathcal{B}}^{hard} = \mathcal{F} \, {}_2F_2\left(1, 1; 2, \frac{3}{2}; \frac{1}{2}\mathcal{F}\right) \quad (30)$$

$$\mathcal{F}_{\mathcal{C}}^{hard} = \mathcal{F} \, {}_2F_2\left(1, 1; 2, \frac{3}{2}; \frac{C_A}{4C_F}\mathcal{F}\right) \quad (31)$$

where \mathcal{F} is the one-loop hard form factor given in Eq. 22.

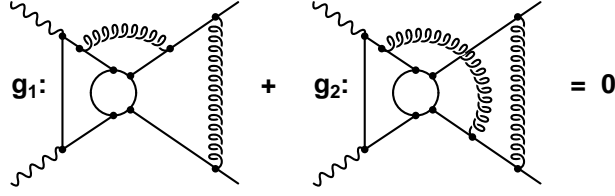


Figure 8: A typical pair of three loop diagrams for topology \mathcal{B} which vanishes in the DL-approximation when both contributions of a gluon radiated off a loop left of the hard blob couples to the outgoing fermion (g_1) and the one coupling to the outgoing anti-fermion (g_2) line are added. The origin of this cancellation, which proceeds to all orders, is the spinor line minus sign of the anti-fermion. Details are discussed in the text.

4.3 Mixed Form Factors

While the novel hard logarithms of the previous section are the most interesting new feature of the $J_z = 0$ $\gamma + \gamma \rightarrow q + \bar{q}$ process, technically the mixed hard and soft contributions are a considerable challenge. In fact for topology \mathcal{C} we are only able to show numerically through three loops that the same structure emerges as for topology \mathcal{B} .

4.3.1 Topology \mathcal{B}

We therefore start with the diagrams given in Fig. 13 for topology \mathcal{B} which contain a soft (s) contribution. The diagram s_5 is evidently given by the product of the two-loop purely hard and the one-loop Sudakov form factors. Also for the sum of diagrams $s_1 + \dots + s_4$, it can easily be seen that we again have a factorization, this time the purely hard one-loop times the two-loop Sudakov form factor.

The nice feature of this topology is that corrections connecting the original one-loop hard form factor with gluon insertions between the outgoing fermions vanish in pairs. The reason is simply a relative spinor line minus sign when a gluon starting from a fermion line of the original one-loop topology is connected with one of the final state fermions. One always has in this case an analogous correction which ends on the anti-fermion line, thus yielding a relative minus sign. Fig. 8 indicates the cancellation in pairs. In this particular case, for instance, we find (choosing the Sudakov parametrization $\{k_1, (p_1 - \frac{m^2}{s}k_1)\}$ for g_1 and $\{k_1, (p_2 - \frac{m^2}{s}k_1)\}$ for g_2 with respect to the gluon going across the hard blob):

$$\Theta_{g_1} \sim -\Theta(s\alpha\beta - m^2) \Theta(s\alpha_1\beta_1 - \lambda^2) \Theta(s\alpha_2\beta_2 - \lambda^2) \Theta\left(\alpha_1 - \frac{m^2}{s}\beta_1\right)$$

$$\times \Theta\left(\beta_1 - \frac{m^2}{s}\alpha_1\right) \Theta\left(\beta_2 - \frac{m^2}{s}(\alpha_2 - \beta_1)\right) \Theta(\alpha_2 - \alpha) \Theta(\beta_2 - \alpha_1) \quad (32)$$

$$\begin{aligned} \Theta_{g_2} &\sim \Theta\left(s\alpha\beta - m^2\right) \Theta\left(s\alpha_1\beta_1 - \lambda^2\right) \Theta\left(s\alpha_2\beta_2 - \lambda^2\right) \Theta\left(\alpha_1 - \frac{m^2}{s}\beta_1\right) \\ &\times \Theta\left(\beta_1 - \frac{m^2}{s}\alpha_1\right) \Theta\left(\beta_2 - \frac{m^2}{s}(\alpha_2 - \alpha_1)\right) \Theta(\alpha_2 - \alpha) \Theta(\beta_2 - \beta_1) \quad (33) \end{aligned}$$

The g_2 contribution is minus that of g_1 after the replacement $\alpha_1 \longleftrightarrow \beta_1$ has been made. The two diagrams therefore cancel each other. This feature holds to all orders and thus leads to a product of the hard form factor in Eq. 30 and the Sudakov form factor in Eq. 23. In other words we have

$$\mathcal{F}_B^{hs} = \mathcal{F} \, {}_2F_2\left(1, 1; 2, \frac{3}{2}; \frac{1}{2}\mathcal{F}\right) [\exp(\mathcal{F}_A) - 1] \quad (34)$$

where we have again used the notation introduced in section 3 for the one-loop form factors. hs refers to the mixed hard (h) and soft (s) nature of the form factor.

4.3.2 Topology \mathcal{C}

For the diagrams given in Figs. 14 and 15 there is no obvious way of generalizing a cancellation between diagrams to all orders. We therefore chose to calculate these corrections explicitly through three loops and compare with the “expected” analogous result found for topology \mathcal{B} in Eq. 34. The results are given in appendix A. Fig. 9 shows a comparison of the contribution from the second term of the hard form factor from Eq. 31 multiplied by the one-loop soft form factor of Eq. 21 with the three loop corrections given by $s_{13} + \dots s_{20}$ in Fig. 14. Only the diagrams $s_{13} + s_{14} + s_{15}$ actually contribute, the others are either zero (s_{19} and s_{20}) or cancel in the sum ($s_{16} + s_{17} + s_{18} = 0$) in the DL-approximation. The leading logarithmic behavior is shown to agree for both $\lambda \rightarrow 0$ as well as for $s \rightarrow \infty$, keeping $m = m_b$ fixed. The agreement is better than 1% and improves for large values of the logarithms.

For the other mixed hard and soft contribution at the three loop level, namely the one-loop hard form factor in Eq. 22 multiplied by the second term in the Sudakov exponential of Eq. 23, many more diagrams contribute. The remaining soft diagrams of Figs. 14 and 15 are not only more numerous but also contain technical subtleties worth mentioning.

In particular, diagrams containing a soft gluon radiating off the “soft” fermion line facing the hard blob need careful consideration. In those cases one has two (for

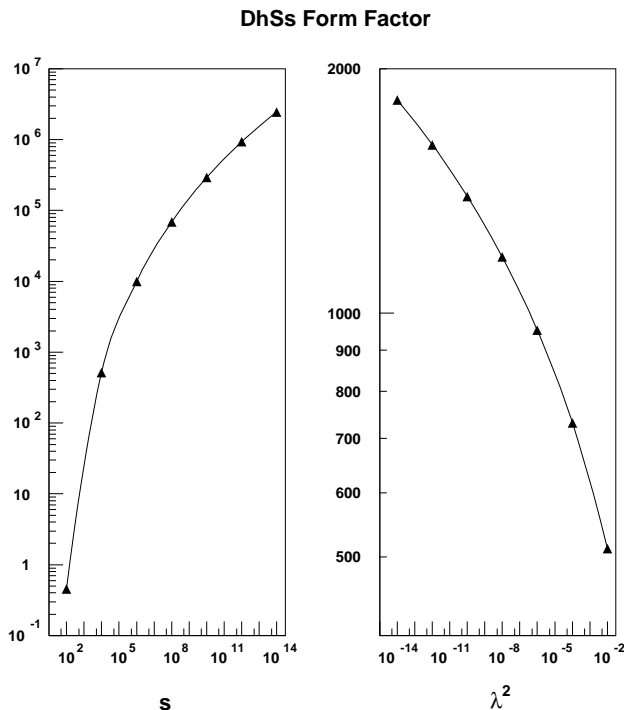


Figure 9: A comparison of the third term of the series expansion in Eq. 37 (line) with a double hard and single soft form factor (DhSs) and the explicit three loop results given in appendix A.1.2 (triangles). The plot on the left keeps $\lambda^2 = 10^{-2}$ fixed, the one on the right has $s = (100 \text{ GeV})^2$ for each data point. For the three loop results we used 10^6 evaluations for each of the 100 iterations and $m_b = 4.5 \text{ GeV}$ was used in both plots. The absolute values are plotted and the agreement is below the percent level. Color factors and the coupling constant are omitted.

diagrams s_{11} and s_{12} of Fig. 14 even three) regions in the phase space contributing to the DL-corrections, corresponding to either side of the “soft” fermion line going on shell.

For instance the two loop diagram in Fig. 10 possesses this ambiguity. It actually does not give a contribution in the DL-approximation due to an asymmetry of the diagram with respect to the external momenta $\{k_2, p_2\}$, while the large variables (see Eq. 11) do not differ in the DL-approximation if we make the replacement $k_2 \longleftrightarrow p_2$. The three loop diagrams s_{19} and s_{20} in Fig. 14 vanishes for the same reason. The easiest way to see this on a technical level is therefore to parametrize l_1 choosing $\{k_2, p_2\}$ for the Sudakov decomposition. Expanding around the left side of the “soft” fermion line in Fig. 10 we find:

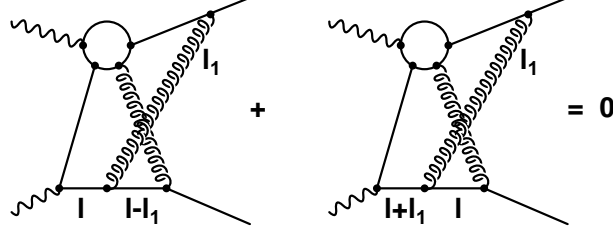


Figure 10: A two loop diagram for topology \mathcal{C} which vanishes in the DL-approximation when both contributions of the soft fermion momentum l to the left and right of the gluon insertion are treated properly. As there is no “obvious” choice for the Sudakov parametrization of the gluon momentum, technical difficulties can arise. Details are discussed in the text.

$$\begin{aligned} \Theta_1 \sim & \Theta(s\alpha\beta - m^2) [\Theta(\beta_1 - \alpha_1) \Theta(\beta - \beta_1) \Theta(\alpha_1\beta - \alpha\beta_1 - \alpha\beta - \alpha_1\beta_1) \\ & + \Theta(\alpha_1 - \beta_1) \Theta(\beta - \beta_1) \Theta(\alpha\beta_1 - \alpha_1\beta - \alpha\beta - \alpha_1\beta_1)] \end{aligned} \quad (35)$$

Shifting the fermion loop momentum, effectively $l \rightarrow l+l_1$, and expanding around the right side of the gluon insertion gives analogously:

$$\begin{aligned} \Theta_2 \sim & -\Theta(s\alpha\beta - m^2) [\Theta(\alpha_1 - \beta_1) \Theta(\alpha - \alpha_1) \Theta(\alpha\beta_1 - \alpha_1\beta - \alpha\beta - \alpha_1\beta_1) \\ & + \Theta(\beta_1 - \alpha_1) \Theta(\alpha - \alpha_1) \Theta(\alpha_1\beta - \alpha\beta_1 - \alpha\beta - \alpha_1\beta_1)] \end{aligned} \quad (36)$$

where we have omitted the common color factor. The second contribution is evidently ($-$) the first after the replacements $\alpha \leftrightarrow \beta$ and $\alpha_1 \leftrightarrow \beta_1$. For the soft contributions of the three loop diagrams $s_5, s_6, s_9, s_{10}, s_{11}$ and s_{12} where the antisymmetry is removed by the additional gluon, we find it technically more convenient to choose $\{k_2, p_1\}$ for the Sudakov decomposition for the genuine DL-corrections listed in appendix A. A careful treatment should in any case give the same result, however.

Fig. 11 shows that the three loop contribution of the sum of diagrams $s_1 + \dots + s_{12}$ is indeed equal to the product of the one-loop hard form factor in Eq. 22 multiplied by the second term in the Sudakov exponential of Eq. 23. The leading logarithmic behavior is shown to agree for both $\lambda \rightarrow 0$ as well as for $s \rightarrow \infty$, keeping $m = m_b$ fixed. The relative difference actually decreases with increasing values of the large logarithms.

It is therefore more than suggestive that the structure which prevails for the one-, two- and three-loop DL-contributions exponentiates to all orders analogously to that of topology \mathcal{B} in Eq. 34, namely that

$$\mathcal{F}_c^{hs} = \mathcal{F} \, {}_2F_2(1, 1; 2, \frac{3}{2}; \frac{C_A}{4C_F} \mathcal{F}) [\exp(\mathcal{F}_A) - 1] \quad (37)$$

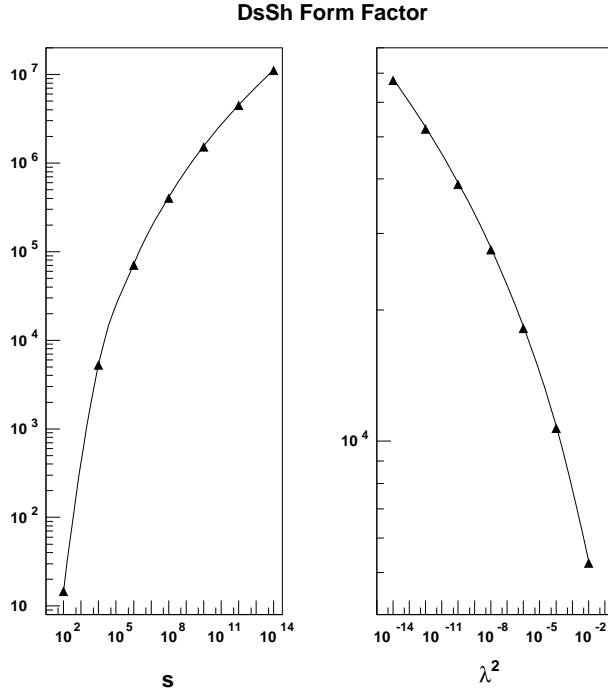


Figure 11: A comparison of the third term of the series expansion in Eq. 37 (line) with a double soft and single hard form factor (DsSh) and the explicit three loop results given in appendix A.1.1 (triangles). The plot on the left keeps $\lambda^2 = 10^{-2}$ fixed, the one on the right has $s = (100 \text{ GeV})^2$ for each data point. For the three loop results we used 10^6 evaluations for each of the 100 iterations and $m_b = 4.5 \text{ GeV}$ was used in both plots. The absolute values are plotted and the agreement is below the percent level. Color factors and the coupling constant are omitted.

5 Summary

In this paper we have derived a novel series of hard double logarithms in polarized $\gamma\gamma$ ($J_z = 0$) collisions to all orders. The resulting series is given by a confluent hypergeometric function ${}_2F_2$ which possesses a $\log\left(\frac{\alpha_s}{\pi} \log^2 \frac{m^2}{s}\right)$ high energy limit. Taking into account the $\frac{m}{\sqrt{s}}$ suppression contained in the Born amplitude, the new corrections are well behaved as $s \rightarrow \infty$. The series expansion agrees with the known one and two loop results as well as our explicit three loop calculation.

It was furthermore shown that at three loops all additional doubly logarithmic corrections are described by the exponentiation of Sudakov logarithms at each order in the expansion of the new hard form factor. This behavior is already present at one and two loops and can thus safely be extrapolated to all orders.

In summary we list the complete virtual DL-form factor contribution to the process $\gamma + \gamma (J_z = 0) \rightarrow q + \bar{q}$:

$$\begin{aligned}
\mathcal{M}_{DL} &= \mathcal{M}_{Born} \left\{ \exp(\mathcal{F}_A) + \mathcal{F} \, {}_2F_2\left(1, 1; 2, \frac{3}{2}; \frac{1}{2}\mathcal{F}\right) + 2 \mathcal{F} \, {}_2F_2\left(1, 1; 2, \frac{3}{2}; \frac{C_A}{4C_F}\mathcal{F}\right) \right. \\
&\quad \left. + \mathcal{F} \, {}_2F_2\left(1, 1; 2, \frac{3}{2}; \frac{1}{2}\mathcal{F}\right) [\exp(\mathcal{F}_A) - 1] \right. \\
&\quad \left. + 2 \mathcal{F} \, {}_2F_2\left(1, 1; 2, \frac{3}{2}; \frac{C_A}{4C_F}\mathcal{F}\right) [\exp(\mathcal{F}_A) - 1] \right\} \\
&= \mathcal{M}_{Born} \left\{ 1 + \mathcal{F} \, {}_2F_2\left(1, 1; 2, \frac{3}{2}; \frac{1}{2}\mathcal{F}\right) + 2 \mathcal{F} \, {}_2F_2\left(1, 1; 2, \frac{3}{2}; \frac{C_A}{4C_F}\mathcal{F}\right) \right\} \exp(\mathcal{F}_A)
\end{aligned} \tag{38}$$

where \mathcal{F}_A and \mathcal{F} denote the soft and hard one-loop form factors of Eqs. 21 and 22 respectively. It should be pointed out that the contributions containing the soft form factor \mathcal{F}_A cancel in a physical cross section with the infrared divergent contributions from the emission of real soft gluons. For realistic future collider applications Fig. 5 demonstrated that the higher than second order contributions are important if an accuracy in the percentile regime could be reached. A more thorough study of the phenomenological implications of this work including realistic experimental cuts is in progress [21].

Acknowledgements

The Authors would like to thank M. Wüsthoff for valuable discussions and M. Heysler for helpful advice on using “Paw”. This work was supported in part by the EU Fourth Framework Programme ‘Training and Mobility of Researchers’, Network ‘Quantum Chromodynamics and the Deep Structure of Elementary Particles’, contract FMRX-CT98-0194 (DG 12 - MIHT).

A Three Loop Results in the DL-Approximation

A.1 Hard and Soft Corrections

In this appendix we give explicit three loop results for the Θ_k terms of Eq. 20 of topology \mathcal{C} . The particular contributions are listed in Fig. 14 with the corresponding notation. For the three loop contribution of topology \mathcal{B} in Fig. 13 the left and right side of the hard blob factorize for the graphs s_1, \dots, s_5 . On a technical level they are therefore effectively two loop corrections. See Ref. [7] for explicit results.

In the following we distinguish between corrections with one and those with two purely hard form factors. We also omit color factors at this point, as the exponentiation of the soft gluons ensures that all “higher” order C_A contributions are canceled by purely non-Abelian corrections [16, 15, 17]. The correct color factors of the sum of the graphs given in Figs. 14, 15 and 16 are contained in the results of section 4.

A.1.1 Double Soft Single Hard Contributions

The following results for the Θ_k correspond to the respective graphs of Fig. 14 with two potentially soft gluons. The Sudakov parametrization for the three soft momenta (as indicated in the figure for s_1) was chosen to be $\{k_2, (p_2 - \frac{m^2}{s}k_2)\}$ for the soft fermion line l in all graphs, $\{(p_1 - \frac{m^2}{s}p_2), (p_2 - \frac{m^2}{s}p_1)\}$ for l_1 in s_1, s_2 and for l_2 in s_1, \dots, s_6 and $\{k_2, (p_1 - \frac{m^2}{s}k_2)\}$ for l_1 in s_3, \dots, s_{12} and for l_2 in s_7, \dots, s_{12} .

$$\begin{aligned} \Theta_{s_1} \sim & -\Theta\left(\alpha\beta - \frac{m^2}{s}\right) \Theta\left(\alpha_1\beta_1 - \frac{\lambda^2}{s}\right) \Theta\left(\alpha_1 - \frac{m^2}{s}\beta_1\right) \Theta\left(\beta_1 - \frac{m^2}{s}\alpha_1\right) \\ & \Theta\left(\alpha_2 - \frac{m^2}{s}\beta_2\right) \Theta\left(\beta_2 - \frac{m^2}{s}\alpha_2\right) \Theta(\alpha_2 - \alpha_1) \Theta(\beta_2 - \beta_1) \Theta(\beta - \beta_2) \end{aligned} \quad (39)$$

$$\begin{aligned} \Theta_{s_2} \sim & -\Theta\left(\alpha\beta - \frac{m^2}{s}\right) \Theta\left(\alpha_1\beta_1 - \frac{\lambda^2}{s}\right) \Theta\left(\alpha_2\beta_2 - \frac{\lambda^2}{s}\right) \Theta\left(\alpha_1 - \frac{m^2}{s}\beta_1\right) \\ & \Theta\left(\beta_1 - \frac{m^2}{s}\alpha_2\right) \Theta\left(\alpha_2 - \frac{m^2}{s}\beta_1\right) \Theta\left(\beta_2 - \frac{m^2}{s}\alpha_2\right) \Theta(\alpha_2 - \alpha_1) \Theta(\beta_1 - \beta_2) \\ & \Theta(\beta - \beta_1) \end{aligned} \quad (40)$$

$$\begin{aligned} \Theta_{s_3} \sim & -\Theta\left(\alpha\beta - \frac{m^2}{s}\right) \Theta\left(\alpha_1\beta_1 - \frac{\lambda^2}{s}\right) \Theta\left(\alpha_2\beta_2 - \frac{\lambda^2}{s}\right) \Theta\left(\alpha_1 - \frac{m^2}{s}\beta_1\right) \\ & \Theta\left(\beta_1 - \frac{m^2}{s}\alpha_1\right) \Theta\left(\beta_2 - \frac{m^2}{s}(\alpha_2 + \beta_1)\right) \Theta(\alpha_2 - \alpha) \Theta(\beta_2 - \alpha_1) \Theta(\beta - \beta_1) \end{aligned} \quad (41)$$

$$\begin{aligned} \Theta_{s_4} \sim & -\Theta\left(\alpha\beta - \frac{m^2}{s}\right) \Theta\left(\alpha_1\beta_1 - \frac{\lambda^2}{s}\right) \Theta\left(\alpha_2\beta_2 - \frac{\lambda^2}{s}\right) \Theta\left(\beta_2 - \frac{m^2}{s}\alpha_2\right) \\ & \Theta\left(\beta_1 - \frac{m^2}{s}\alpha_1\right) \Theta\left(\alpha_1 - \frac{m^2}{s}(\alpha_2 + \beta_1)\right) \Theta(\alpha_2 - \alpha) \Theta(\alpha_1 - \beta_2) \Theta(\beta - \beta_1) \end{aligned} \quad (42)$$

$$\begin{aligned} \Theta_{s_5} \sim & -\Theta\left(\alpha\beta - \frac{m^2}{s}\right) \Theta\left(\alpha_1\beta_1 - \frac{\lambda^2}{s}\right) \Theta\left(\alpha_2\beta_2 - \frac{\lambda^2}{s}\right) \Theta\left(\beta_1 - \frac{m^2}{s}\alpha_1\right) \\ & \Theta\left(\alpha_1 - \frac{m^2}{s}\beta_1\right) \Theta(\alpha_2 - \alpha_1) \Theta((\alpha + \beta)\beta_2 - \alpha\alpha_2 - \alpha\beta - \alpha_2\beta_2) \\ & \Theta\left(\alpha_2 - \frac{m^2}{s}(\beta_1 + \beta_2)\right) \{\Theta(\alpha - \beta_2) \Theta(\beta - \beta_1) - \Theta(\beta - \beta_1 - \beta_2 - \alpha_2)\} \end{aligned} \quad (43)$$

$$\begin{aligned} \Theta_{s_6} \sim & -\Theta\left(\alpha\beta - \frac{m^2}{s}\right) \Theta\left(\alpha_1\beta_1 - \frac{\lambda^2}{s}\right) \Theta\left(\alpha_2\beta_2 - \frac{\lambda^2}{s}\right) \Theta\left(\beta_1 - \frac{m^2}{s}\alpha_1\right) \\ & \Theta\left(\beta_2 - \frac{m^2}{s}\alpha_2\right) \Theta(\alpha_1 - \beta_2) \Theta((\alpha + \beta)\alpha_2 - \alpha\beta_2 - \alpha\beta - \alpha_2\beta_2) \end{aligned}$$

$$\Theta\left(\alpha_1 - \frac{m^2}{s}(\beta_1 + \alpha_2)\right) \{\Theta(\alpha - \alpha_2)\Theta(\beta - \beta_1) - \Theta(\beta - \beta_1 - \beta_2 - \alpha_2)\} \quad (44)$$

$$\begin{aligned} \Theta_{s_7} &\sim -\Theta\left(\alpha\beta - \frac{m^2}{s}\right) \Theta\left(\alpha_1\beta_1 - \frac{\lambda^2}{s}\right) \Theta\left(\beta_1 - \frac{m^2}{s}\alpha_1\right) \\ &\Theta\left(\beta_2 - \frac{m^2}{s}\alpha_2\right) \Theta(\alpha_2 - \alpha_1) \Theta(\beta_2 - \beta_1) \Theta(\alpha_1 - \alpha) \end{aligned} \quad (45)$$

$$\begin{aligned} \Theta_{s_8} &\sim -\Theta\left(\alpha\beta - \frac{m^2}{s}\right) \Theta\left(\alpha_1\beta_1 - \frac{\lambda^2}{s}\right) \Theta\left(\alpha_2\beta_2 - \frac{\lambda^2}{s}\right) \Theta\left(\beta_1 - \frac{m^2}{s}\alpha_1\right) \\ &\Theta\left(\beta_2 - \frac{m^2}{s}\alpha_1\right) \Theta(\alpha_2 - \alpha) \Theta(\beta_2 - \beta_1) \Theta(\alpha_1 - \alpha_2) \end{aligned} \quad (46)$$

$$\begin{aligned} \Theta_{s_9} &\sim -\Theta\left(\alpha\beta - \frac{m^2}{s}\right) \Theta\left(\alpha_1\beta_1 - \frac{\lambda^2}{s}\right) \Theta\left(\alpha_2\beta_2 - \frac{\lambda^2}{s}\right) \Theta\left(\beta_2 - \frac{m^2}{s}\alpha_2\right) \\ &\Theta(\beta_1 - \beta_2) \Theta\left(\beta_1 - \frac{m^2}{s}(\alpha_1 + \alpha_2)\right) \Theta((\alpha + \beta)\alpha_2 - \alpha\beta_2 - \alpha\beta - \alpha_2\beta_2) \\ &\Theta(\alpha_1 - \alpha) \{\Theta(\alpha - \alpha_2) - \Theta(\beta - \beta_1 - \alpha_1)\} \end{aligned} \quad (47)$$

$$\begin{aligned} \Theta_{s_{10}} &\sim -\Theta\left(\alpha\beta - \frac{m^2}{s}\right) \Theta\left(\alpha_1\beta_1 - \frac{\lambda^2}{s}\right) \Theta\left(\alpha_2\beta_2 - \frac{\lambda^2}{s}\right) \Theta\left(\beta_1 - \frac{m^2}{s}\alpha_1\right) \Theta(\beta_2 - \beta_1) \\ &\Theta\left(\beta_2 - \frac{m^2}{s}(\alpha_1 + \alpha_2)\right) \Theta((\alpha + \beta)\alpha_2 - \alpha\beta_2 - \alpha\beta - \alpha_2\beta_2) \\ &\Theta(\alpha_1 - \alpha) \{\Theta(\alpha - \alpha_2) - \Theta(\beta - \beta_2 - \alpha_2)\} \end{aligned} \quad (48)$$

$$\begin{aligned} \Theta_{s_{11}} &\sim -\Theta\left(\alpha\beta - \frac{m^2}{s}\right) \Theta\left(\alpha_1\beta_1 - \frac{\lambda^2}{s}\right) \Theta\left(\alpha_2\beta_2 - \frac{\lambda^2}{s}\right) \Theta\left(\beta_1 - \frac{m^2}{s}\alpha_1\right) \Theta(\beta_2 - \beta_1) \\ &\Theta\left(\beta_2 - \frac{m^2}{s}(\alpha_1 + \alpha_2)\right) \\ &\{\Theta(\beta - \beta_1 - \alpha_1 - \beta_2 - \alpha_2) \Theta((\alpha + \beta)\alpha_2 - \alpha\beta_2 - \alpha\beta - \alpha_2\beta_2) \\ &\Theta((\alpha + \beta)\alpha_1 - (\alpha + \beta)\alpha_2 - \alpha\beta_1 - \alpha_1\beta_2 - \alpha_2\beta_1 - \alpha_1\beta_1) - \\ &\Theta(\alpha - \alpha_2) \Theta(\beta - \beta_1 - \alpha_1) \Theta((\alpha + \beta)\alpha_1 - \alpha\beta_1 - \alpha\beta - \alpha_1\beta_1) \\ &\Theta((\alpha + \beta)\alpha_2 - \alpha\beta_2 - \alpha\beta - \alpha_2\beta_2) + \\ &\Theta(\alpha - \alpha_1 - \alpha_2) \Theta((\alpha + \beta)\alpha_2 - (\alpha + \beta)\alpha_1 - \alpha\beta_2 - \alpha_1\beta_2 - \alpha_2\beta_1 - \alpha_2\beta_2) \\ &\Theta((\alpha + \beta)\alpha_1 - \alpha\beta_1 - \alpha\beta - \alpha_1\beta_1)\} \end{aligned} \quad (49)$$

$$\begin{aligned} \Theta_{s_{12}} &\sim -\Theta\left(\alpha\beta - \frac{m^2}{s}\right) \Theta\left(\alpha_1\beta_1 - \frac{\lambda^2}{s}\right) \Theta\left(\alpha_2\beta_2 - \frac{\lambda^2}{s}\right) \Theta\left(\beta_2 - \frac{m^2}{s}\alpha_2\right) \Theta(\beta_1 - \beta_2) \\ &\Theta\left(\beta_1 - \frac{m^2}{s}(\alpha_1 + \alpha_2)\right) \\ &\{\Theta(\beta - \beta_1 - \alpha_1 - \beta_2 - \alpha_2) \Theta((\alpha + \beta)\alpha_1 - \alpha\beta_1 - \alpha\beta - \alpha_1\beta_1) \end{aligned}$$

$$\begin{aligned}
& \Theta((\alpha + \beta) \alpha_2 - (\alpha + \beta) \alpha_1 - \alpha \beta_2 - \alpha_1 \beta_2 - \alpha_2 \beta_1 - \alpha_2 \beta_2) - \\
& \Theta(\alpha - \alpha_1) \Theta(\beta - \beta_2 - \alpha_2) \Theta((\alpha + \beta) \alpha_1 - \alpha \beta_1 - \alpha \beta - \alpha_1 \beta_1) \\
& \Theta((\alpha + \beta) \alpha_2 - \alpha \beta_2 - \alpha \beta - \alpha_2 \beta_2) + \\
& \Theta(\alpha - \alpha_1 - \alpha_2) \Theta((\alpha + \beta) \alpha_1 - (\alpha + \beta) \alpha_2 - \alpha \beta_1 - \alpha_1 \beta_2 - \alpha_2 \beta_1 - \alpha_1 \beta_1) \\
& \Theta((\alpha + \beta) \alpha_2 - \alpha \beta_2 - \alpha \beta - \alpha_2 \beta_2) \} \tag{50}
\end{aligned}$$

A.1.2 Double Hard Single Soft Contributions

Below we give the results for the Θ_k corresponding to the respective graphs of Fig. 14 with one potentially soft gluon. The Sudakov parametrization for the three soft momenta (as indicated in the figure for s_1) was $\{k_2, (p_2 - \frac{m^2}{s} k_2)\}$ for the soft fermion line l and for l_1 in all graphs and for l_2 in s_{16}, \dots, s_{20} , $\{(p_1 - \frac{m^2}{s} p_2), (p_2 - \frac{m^2}{s} p_1)\}$ for l_2 in s_{13} and $\{k_2, (p_1 - \frac{m^2}{s} k_2)\}$ for l_2 in s_{14}, s_{15} .

$$\begin{aligned}
\Theta_{s_{13}} & \sim -\Theta\left(\alpha\beta - \frac{m^2}{s}\right) \Theta\left(\alpha_2\beta_2 - \frac{\lambda^2}{s}\right) \Theta\left(\alpha_2 - \frac{m^2}{s}\beta_2\right) \Theta\left(\beta_2 - \frac{m^2}{s}\alpha_2\right) \\
& \Theta(\beta - \beta_2) \Theta(\alpha_1 - \alpha) \Theta(\beta_1 - \beta) \tag{51}
\end{aligned}$$

$$\begin{aligned}
\Theta_{s_{14}} & \sim -\Theta\left(\alpha\beta - \frac{m^2}{s}\right) \Theta\left(\alpha_2\beta_2 - \frac{\lambda^2}{s}\right) \Theta\left(\beta_2 - \frac{m^2}{s}\alpha_2\right) \\
& \Theta(\alpha_1 - \alpha_2) \Theta(\alpha_2 - \alpha) \Theta(\beta_1 - \beta) \tag{52}
\end{aligned}$$

$$\begin{aligned}
\Theta_{s_{15}} & \sim -\Theta\left(\alpha\beta - \frac{m^2}{s}\right) \Theta\left(\alpha_2\beta_2 - \frac{\lambda^2}{s}\right) \Theta\left(\beta_2 - \frac{m^2}{s}\alpha_2\right) \\
& \Theta(\alpha_2 - \alpha_1) \Theta(\alpha_1 - \alpha) \Theta(\beta_1 - \beta) \tag{53}
\end{aligned}$$

$$\begin{aligned}
\Theta_{s_{16}} & \sim -\Theta\left(\alpha\beta - \frac{m^2}{s}\right) \Theta\left(\alpha_2\beta_2 - \frac{\lambda^2}{s}\right) \Theta\left(\beta_2 - \frac{m^2}{s}\alpha_2\right) \\
& \Theta(\alpha_1 - \alpha) \Theta(\alpha_2 - \alpha) \Theta(\beta_1 - \beta) \Theta(\beta - \beta_2) \tag{54}
\end{aligned}$$

$$\begin{aligned}
\Theta_{s_{17}} & \sim \Theta\left(\alpha\beta - \frac{m^2}{s}\right) \Theta\left(\alpha_2\beta_2 - \frac{\lambda^2}{s}\right) \Theta\left(\beta_2 - \frac{m^2}{s}\alpha_2\right) \\
& \Theta(\alpha_1 - \alpha_2) \Theta(\alpha_2 - \alpha) \Theta(\beta_1 - \beta) \Theta(\beta - \beta_2) \tag{55}
\end{aligned}$$

$$\begin{aligned}
\Theta_{s_{18}} & \sim \Theta\left(\alpha\beta - \frac{m^2}{s}\right) \Theta\left(\alpha_2\beta_2 - \frac{\lambda^2}{s}\right) \Theta\left(\beta_2 - \frac{m^2}{s}\alpha_2\right) \\
& \Theta(\alpha_2 - \alpha_1) \Theta(\alpha_1 - \alpha) \Theta(\beta_1 - \beta) \Theta(\beta - \beta_2) \tag{56}
\end{aligned}$$

$$\Theta_{s_{19}} \sim 0 \tag{57}$$

$$\Theta_{s_{20}} \sim 0 \tag{58}$$

The last two diagrams vanish in the DL-approximation for the same reason as the two loop contribution given in Fig. 10. The diagrams s_{16}, \dots, s_{18} cancel each other after writing

$$\Theta(\alpha_1 - \alpha) \Theta(\alpha_2 - \alpha) = \Theta(\alpha_1 - \alpha_2) \Theta(\alpha_2 - \alpha) + \Theta(\alpha_2 - \alpha_1) \Theta(\alpha_1 - \alpha) \quad (59)$$

Strictly speaking, the above cancellation takes place only for the $C_F^2 C_A$ terms of amplitude s_{18} . The $C_F C_A^2$ term, absent in graphs s_{16} and s_{17} of Fig. 14, is canceled by the analogous contribution of graphs s_{21} and s_{22} of Fig. 15.

In the same way the above mentioned cancellation of “higher order” C_A terms takes place with all non-Abelian graphs of Fig. 15. The remaining diagrams of topology \mathcal{C} in Fig. 16 all cancel among themselves in groups of two or three.

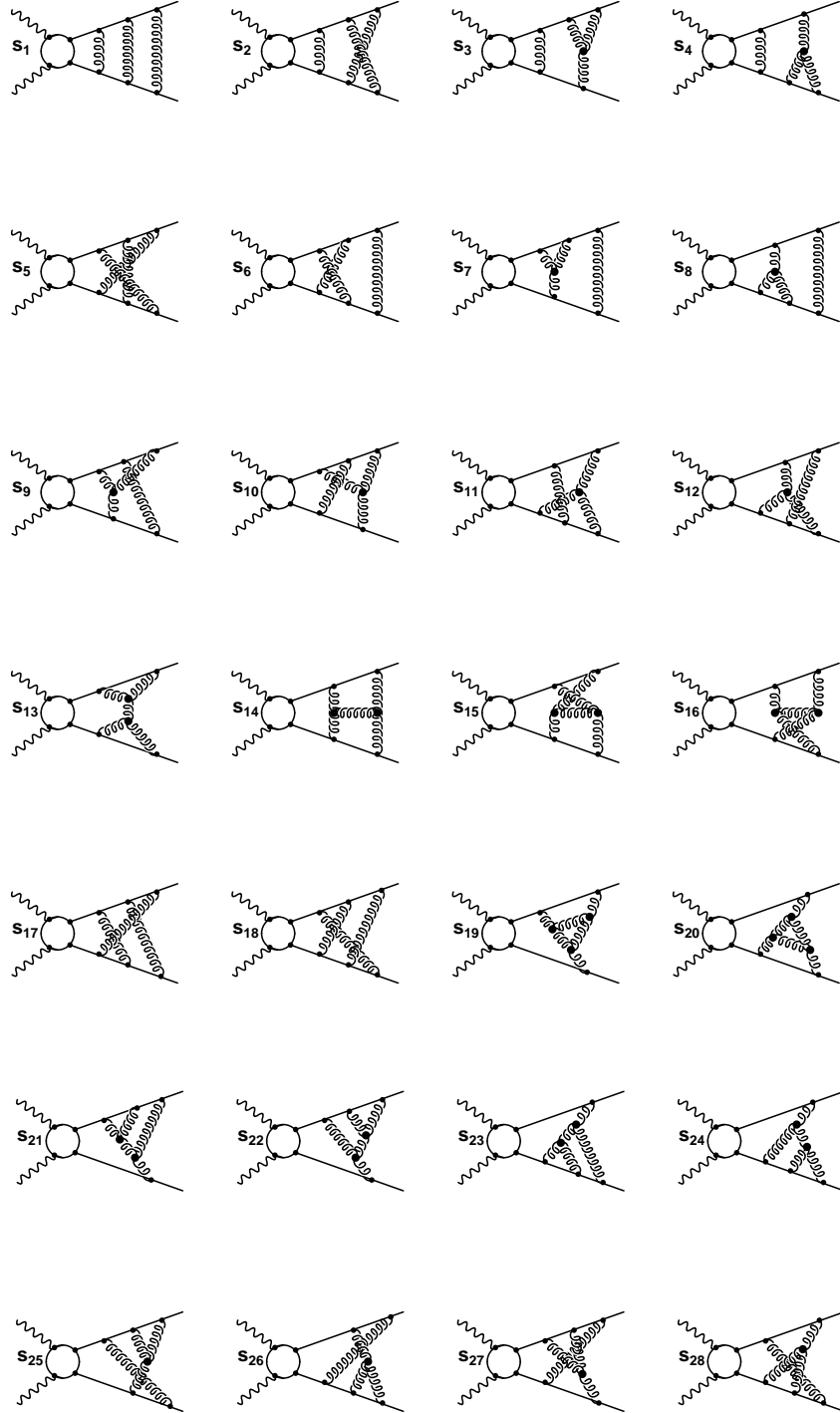


Figure 12: The three loop Feynman diagrams contributing to the purely soft form factor of the topology \mathcal{A} . The sum of all terms exponentiates as usual with the non-Abelian diagrams canceling the C_A parts of the crossed “Abelian” graphs.

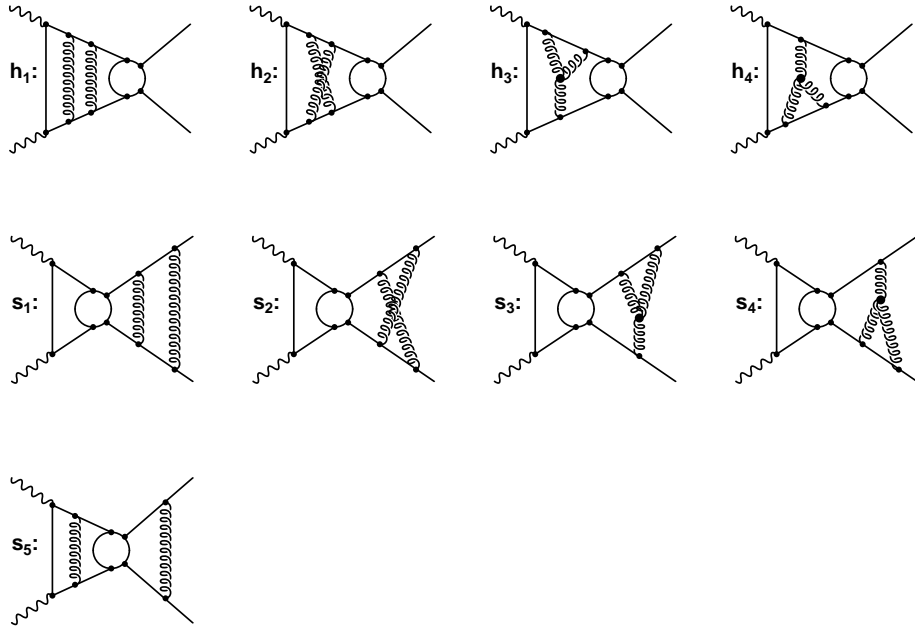


Figure 13: The three loop Feynman diagrams contributing to the purely hard (h) and soft (s) form factors of the topology \mathcal{B} . The sum of all soft terms exponentiates from each order of the hard process. The remaining diagrams cancel pairwise as described in section 4.

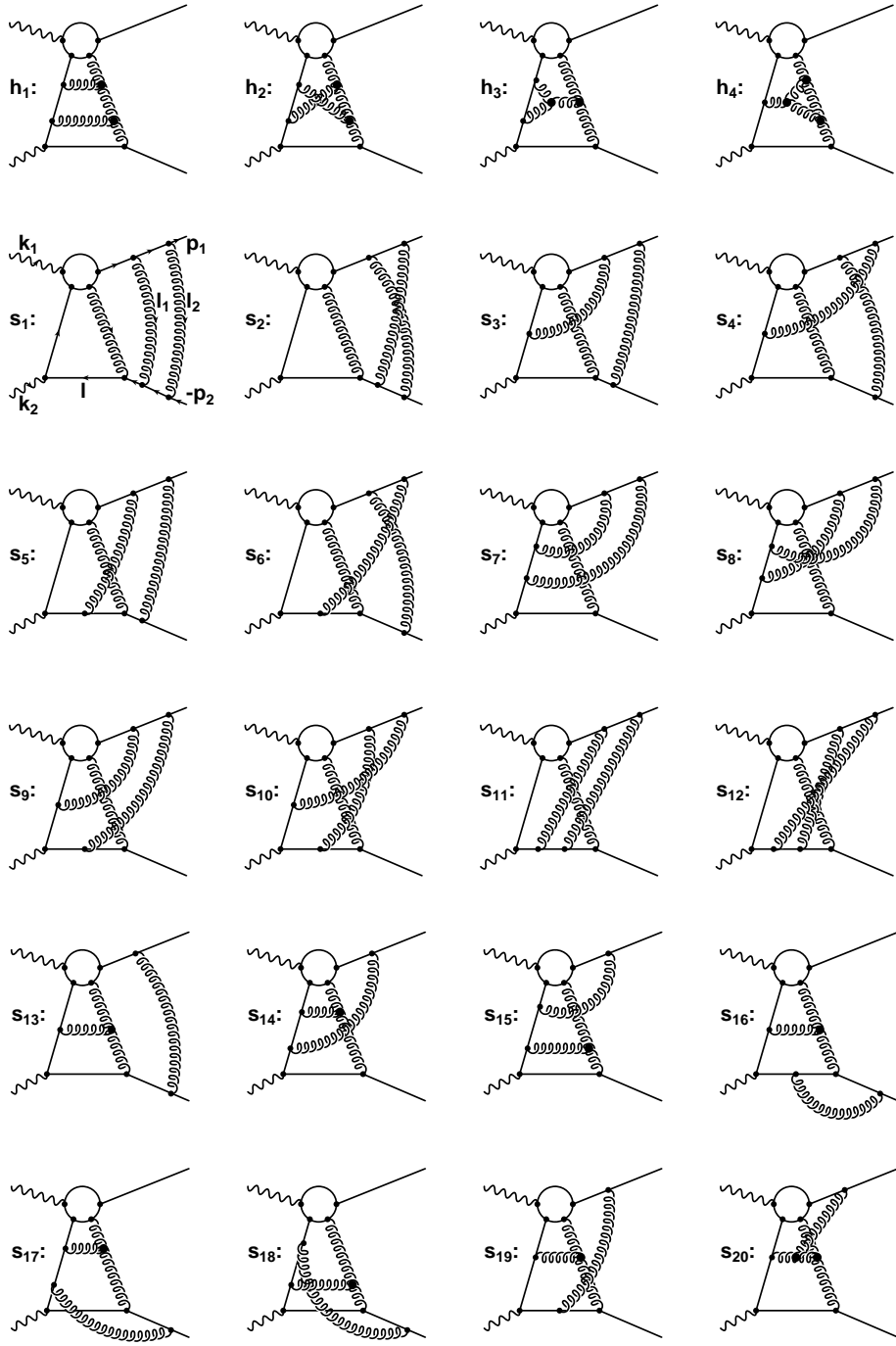


Figure 14: The three loop Feynman diagrams contributing to the hard (h) and soft (s) form factors of the topology \mathcal{C} . The sum of all soft terms exponentiates from each order of the hard process.

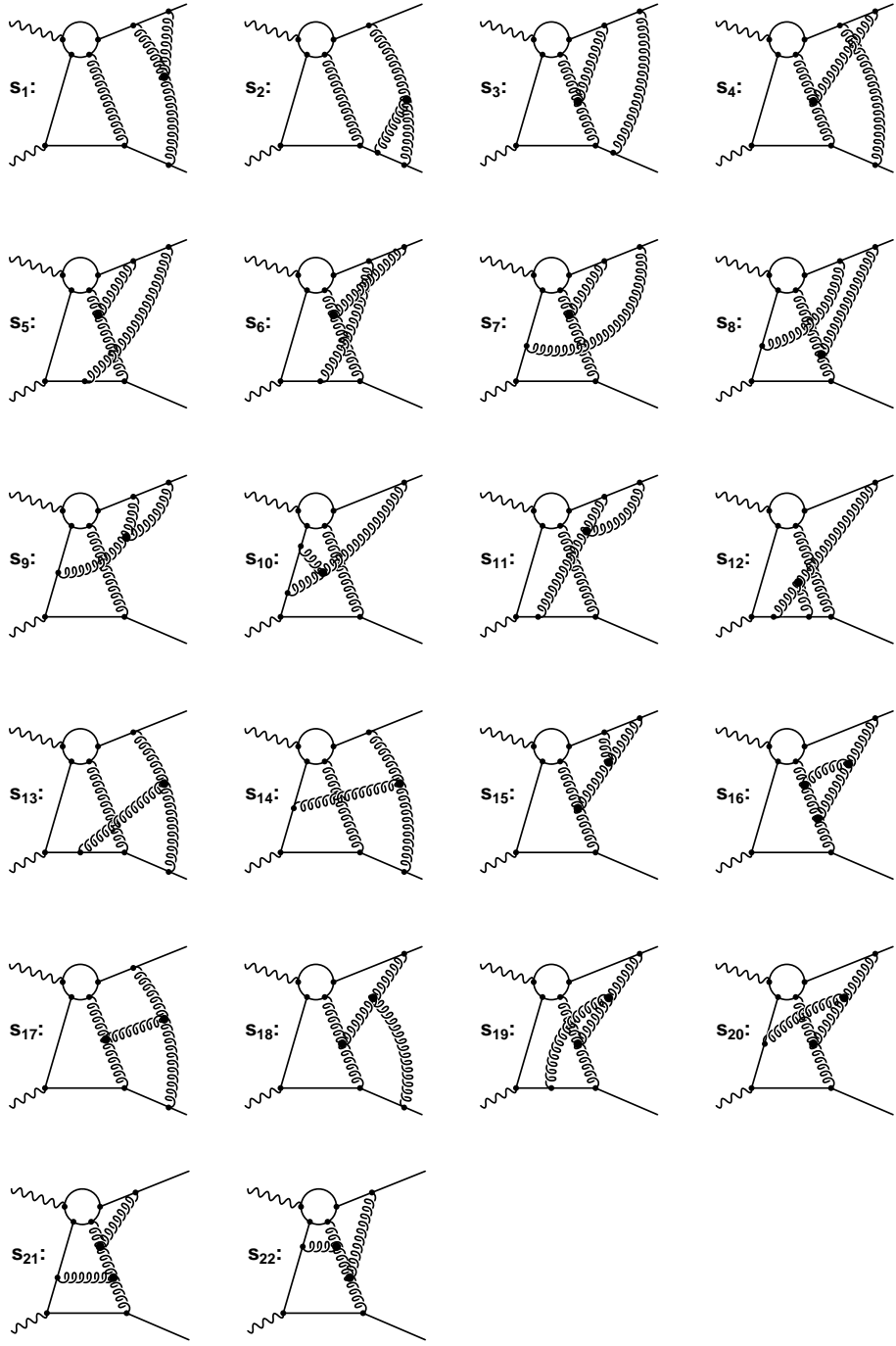


Figure 15: The non-Abelian three loop Feynman diagrams of the topology \mathcal{C} which cancel the C_A parts of color factors occurring in the soft contributions of Fig. 14.

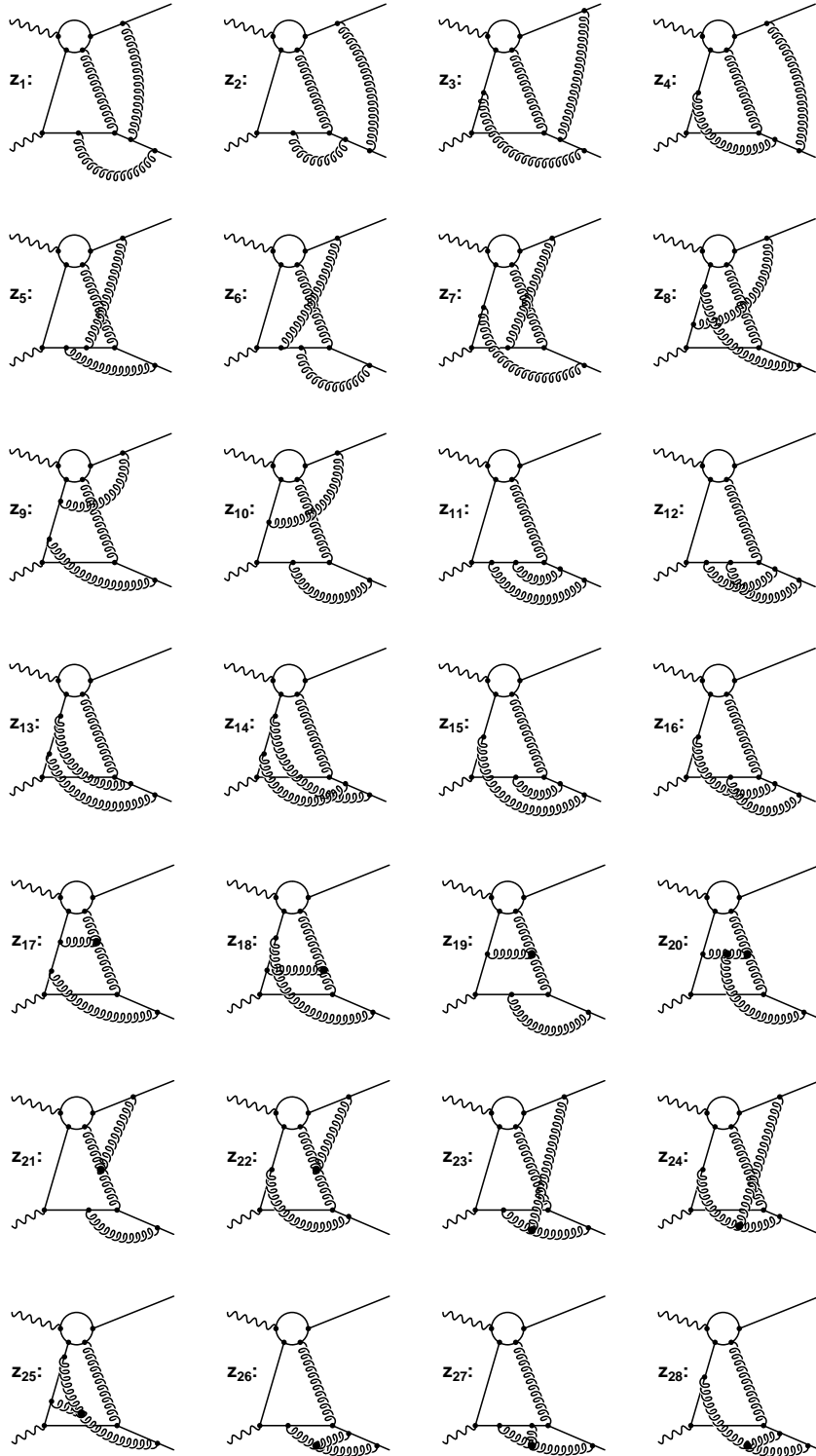


Figure 16: The three loop Feynman diagrams of the topology \mathcal{C} which cancel either pairwise or in groups of three in the leading logarithmic approximation.

References

- [1] I.F. Ginzburg et al., Nucl. Inst. Meth. **205** (1983) 47.
- [2] I.F. Ginzburg et al., Nucl. Inst. Meth. **219** (1984) 5.
- [3] V.I. Telnov, Nucl. Inst. Meth. **A 355** (1995) 5.
- [4] D.L. Borden, V.A. Khoze, J. Ohnemus and W.J. Stirling, Phys. Rev. **D 50** (1994) 4499.
- [5] G. Jikia, A. Takabladze, Phys. Rev. **D 54** (1996) 2030.
- [6] G. Jikia, A. Takabladze, Nucl. Inst. Meth. **A 355** (1995) 81.
- [7] V.S. Fadin, V.A. Khoze and A.D. Martin, Phys. Rev. **D 56** (1997) 484.
- [8] R. Kleiss, W.J. Stirling, Nucl. Phys. **B 262** (1985) 235.
- [9] Landau, Lifshitz, Quantum Electrodynamics, Vol. 2, Pergamon Press, Oxford (1975).
- [10] V.G. Gorshkov, V.N. Gribov, L.N. Lipatov and G.V. Frolov, Sov. J. Nucl. Phys. **6** (1967) 95.
- [11] R. Kirschner, L.N. Lipatov, Nucl. Phys. **B 213** (1983) 122.
- [12] J. Bartels, B.I. Ermolaev and M.G. Ryskin Z. Phys. **C 70** (1996) 627.
- [13] B.I. Ermolaev, S.I. Manayenkov and M.G. Ryskin Z. Phys. **C 69** (1996) 259.
- [14] V.V. Sudakov, Sov. Phys. JETP **3** (1956) 65.
- [15] H.D. Dahmen, F. Steiner, Z. Phys. **C 11** (1981) 247.
- [16] J.M. Cornwall, G. Tiktopoulos, Phys. Rev. **D 13** (1976) 3370.
- [17] A. Sen, Phys. Rev. **D 24** (1981) 3281.
- [18] V.V. Belokurov, N.I. Ussyukina, Phys. Lett. **94 B** (1980) 251.
- [19] Gradshteyn, Ryzhik, Table of Integrals, Series and Products, Academic Press (1994).
- [20] P. Lepage, VEGAS, a Monte Carlo integrator, freely available, (c) (1975), Cornell University.
- [21] M. Melles, W.J. Stirling, in preparation.

